

# A statistical approach for identifying factors governing streamflow recession behaviour

Hongyi Li  | Ali Ameli 

Department of Earth, Ocean and Atmospheric Sciences, The University of British Columbia, Vancouver, British Columbia, Canada

## Correspondence

Ali Ameli, Department of Earth, Ocean and Atmospheric Sciences, The University of British Columbia, Vancouver, BC V6T 1Z4, Canada.

Email: [aameli@eoas.ubc.ca](mailto:aameli@eoas.ubc.ca)

## Funding information

NSERC-Funded Canadian Statistical Science Institute (CANSSI)

## Abstract

Catchment storage-release relation has been widely studied using the parameters of streamflow recession analysis. The governing factors of the recession parameters are poorly understood, particularly in snow-dominated regions. Here, we tailor a newly developed statistical approach, marginal contribution feature importance, to a hydrologic context, and couple it with random forests, in order to investigate the governing physical and climatic factors of catchment recession behaviour. The coupled approach can incorporate the interactions among catchment climatic and physical attributes. In a large sample hydrology study, we identify and compare the governing factors of recession parameters, in rainfall versus snowmelt-dominated catchments, and in medium-size versus large catchments, across more than 1000 catchments in United States and Canada. Results show that streamflow recession behaviour, particularly recession nonlinearity, strongly depend on belowground attributes and slope in rain-dominated medium size catchments, and strongly depend on slope and annual maximum snow water equivalent in snow-dominated medium size catchments. As catchment scale increases ( $>1000 \text{ km}^2$ ), the attributes related to the magnitude and timing of input water (e.g., water surplus, aridity index, maximum snow water equivalent) dictates the streamflow recession behaviour and the importance of below-ground attributes is dropped. Furthermore, recession nonlinearity generally increases with an increase in catchment size. The findings of this study help improve our understanding of the governing factors and the interpretation of the spatial variability of recession behaviours. Such understanding could inform the development of a generalizable process-based framework for estimating the sensitivity of catchment storage-release relation to climate change in different environmental settings.

## KEY WORDS

catchment hydrologic function, hydrograph recession parameters, large sample hydrology, prediction in ungauged basins, random forests, statistical feature importance, storage-release relation, streamflow recession nonlinearity

## 1 | INTRODUCTION

Stream low flow sustains basic summer agricultural needs, describes aquatic habitat during dry seasons (May & Lee, 2004), and prevents saltwater intrusions in coastal catchments (Jasechko et al., 2020).

Understanding stream low flow response in the context of climate change is essential for the different sectors of water resources management since both anthropogenic societies and ecological environments are highly dependent on steady water supply during dry periods (Godsey et al., 2014). Hydrograph recession analysis,

introduced by Brutsaert and Nieber (1977), provides a mechanistic catchment-scale linkage between subsurface storage and subsurface water release during stream low flow and average flow periods (Harman et al., 2009; Troch et al., 2013), and informs stream low flow and average flow vulnerabilities to subsurface storage changes (e.g., Berghuijs et al., 2016; Buttle, 2018; Kirchner, 2009). In order to understand the storage-release processes during low flow and average flow, the physical and climatic drivers of the hydrograph recession and of the mechanistic linkages between subsurface storage and release should be determined in different types of environmental and climatic settings (Blöschl et al., 2014). Understanding these drivers is essentially important as climatic characteristics, particularly snow related attributes, could be impacted by future climate change (Berghuijs et al., 2016; Harpold et al., 2015; Harpold & Brooks, 2018; Musselman et al., 2017). This study develops a statistical framework to identify the physical and climatic drivers of the hydrograph recession, across a wide spectrum of rain to snow-dominated catchments.

The parameters of hydrograph recession have been studied comparatively in several catchments in Europe and North America (e.g., Berghuijs et al., 2016; Buttle, 2018). In these studies, periods without precipitation (i.e., streamflow recession periods) had streamflow hydrographs that displayed a power law decay with a tight linkage to subsurface storage. In these recession periods, streamflow ( $Q$ ) and the time derivative of streamflow ( $-dQ/dt$ ) are related by Equation (1) (Brutsaert & Nieber, 1977):

$$-\frac{dQ}{dt} = aQ^b \quad (1)$$

$b$  and  $a$  are parameters of the power law decay of hydrograph recession, where  $b$  refers to recession nonlinearity and  $\log(a)$  could depict recession instability. Recession nonlinearity ( $b$ ) determines the curvature of the receding limb of the streamflow hydrograph, where a larger  $b$  value means a larger curvature (convexity) of recession curve. We adopt the term “recession instability” from Tashie et al. (2020b). Here, (in)stability refers to how stable the stream can maintain the flow rate during a recession event. For two hypothetical hydrograph recession curves with the same  $Q_0$  (initial recession flow rate) and same  $b$  values, the hydrograph with a larger  $\log(a)$  or  $a$  will always have a lower flow rate than the one with a smaller  $\log(a)$  or  $a$ . Indeed, a larger  $\log(a)$  or  $a$  corresponds to a smaller subsurface storage capacity, implying a smaller flow rate and smaller cumulative flow rate (or comparatively more instable streamflow) at any time during recession.

Theoretical studies related to hydraulic groundwater theory have shown that  $\log(a)$  is controlled by saturated hydraulic conductivity, drainable porosity, aquifer depth, catchment stream length and evapotranspiration, while vertical heterogeneity, hillslope steepness, evapotranspiration, antecedent catchment wetness affect  $b$  (see the review paper by Troch et al., 2013). On the other hand, theoretical and experimental studies conducted by Harman et al. (2009) and Clark's et al. (2009) hypothesized that the spatial (or within-catchment lateral) heterogeneity of catchment physical attributes could be an important

driver of parameter  $b$ . They also depicted that as the catchment size increases, recession nonlinearity increases. Tashie's et al. (2020b) large sample hydrology study across the United states showed that seasonal climatic attributes, catchment storage and lagged evapotranspiration controloled recession instability across (mostly) rain-dominated catchments. They pointed out that the drivers of parameter  $b$  are challenging to identify.

Notable achievements have been made on identifying the drivers of hydrograph recession parameters as explained above. However, it is still not clear whether the climatic and physical drivers of recession parameters differ between snow-dominated and rain-dominated catchments. Furthermore, previous studies did not generally assess the importance of detailed characteristics of snow storage (e.g., timing and magnitude of snow depth) or rainfall (e.g., rainfall intensity) on recession parameters, and focused mostly on the climatic attributes describing the overall water balance of catchments (e.g., total precipitation). In addition, the potentially strong, hydrologically relevant interactions among detailed snow storage or rainfall characteristics and physical attributes were not sufficiently acknowledged in the previous studies, which focused on identifying the dominant drivers of recession parameters. Recent research showed that snow storage or rainfall characteristics and their interactions with catchment physical attributes could control subsurface storage and streamflow generation mechanisms (Janssen & Ameli, 2021; Wu et al., 2021). Resolving these critically important gaps is crucial as climate change is expected to alter the precipitation type, as well as to alter the rate and timing for both snow storage and rainfall (Berghuijs et al., 2014; Clow, 2010; Hammond et al., 2018; Hammond et al., 2019; Woo et al., 2008), while the attributes describing the overall water balance of catchments (e.g., total precipitation) may still remain almost unchanged (McCabe et al., 2018).

Here, we adopt a newly developed statistical approach, Marginal Contribution Feature Importance (Catav et al., 2020), and couple it with random forests, in order to evaluate and rank the influences of a suite of climatic and physical attributes on streamflow recession behaviours in more than 1000 catchments spanning a wide range of climatic, geological (surficial and bedrock), and topographical settings across the United States and Canada. Our climatic attributes include the attributes that show both the overall water balance of catchments and detailed rainfall and snow storage characteristics. We explore the relative importance of a given attribute after accounting for the interactions between the attribute and all other attributes, in rainfall versus snow-dominated catchments, as well as in medium-size versus large catchments.

Specifically, this paper uses a large sample hydrology approach and responds to calls made by Harman et al. (2009) and Clark's et al. (2009) studies, to explore:

1. How do climatic and physical drivers of streamflow recession behaviour vary between snowmelt and rainfall dominated catchments?
2. To what extent does the spatial (or within-catchment lateral) heterogeneity of catchment's physical attributes (e.g., soil hydraulic conductivity) control streamflow recession behaviour?

3. Do the drivers of streamflow recession behaviour vary by catchment size?

The estimation of recession behaviours in ungauged catchments, requires a process-based framework able to analyse globally available catchment data in order to predict streamflow recession parameters, as suggested by Troch et al. (2013) and Clark et al. (2009). Several process-based frameworks have been suggested for predicting streamflow recession parameters using different types of “bottom up” approaches (e.g., Ding et al., 2021; Luo et al., 2018; Rupp & Selker, 2005; Rupp & Selker, 2006). These include (among others): one-dimensional saturated representation of a hillslope, developed by Troch et al. (2003), three-dimensional Richards Equation based numerical model developed by Paniconi et al. (2003) or linearized hillslope-storage Boussinesq model (hsB) which was solved analytically (e.g., Dralle et al., 2014) and numerically (e.g., Hazenberg et al., 2015). More recently, Ranjram and Craig (2021) developed a proxy solution for the hsB model that can upscale and solve a network of heterogenous hillslopes, using a hybrid numerical-probabilistic approach, in order to estimate catchment-scale recession parameters. Given the large data requirement for bottom-up process-based approaches, here we employ a “top-down” large sample hydrology empirical path that relies solely on globally available data and prioritizes generalization and simplification in model design (McDonnell et al., 2007). In addition to the above-mentioned objectives, we develop a random forests tool in order to predict recession parameters using process-motivated catchment-scale attributes (e.g., snow storage, rainfall intensity). We evaluate the performance of this machine learning model across a spectrum of gauged to poorly-gauged regions. We consider this attempt as a small step toward developing generalizable tools for the prediction of storage-release relations, and recession behaviours, in ungauged regions.

## 2 | DATA

### 2.1 | Streamflow data

Our initial streamflow data consist of 2273 gauges across Canada and the United States. We obtained 1602 Canadian gauges from the HYDAT dataset released by the Water Survey Canada and 671 United States stream gauges from the CAMELS dataset (Addor et al., 2017). We excluded 1240 of them where one or more of these conditions applied:

1. Catchments for which we were unable to identify at least 25 recession events during its available record range. This threshold is set to ensure that the estimated recession parameters are robust and are not biased to a few potentially irregular individual recession events, and in the meantime keep a sufficient number of catchments to ensure the subsequent statistical study had a meaningful sample size.

2. Catchments with areas smaller than 50 km<sup>2</sup>. Small catchments were excluded due to uncertainty caused by the coarse resolution of climatic attributes, in a manner similar to Janssen and Ameli (2021) and Wu et al. (2021).
3. Catchments having more than 10% of days with missing streamflow data during each year of hydrologic years between 1981 and 2019.
4. Canadian catchments in which the estimated area (using the Watershed Tool in ArcGIS; see Section 2.3.1) and computed area (using Water Survey Canada topographic maps) differed by more than 30%. We applied this filter, in a manner similar to Addor et al. (2017), as a large discrepancy in calculated areas (and boundary polygons) of a catchment between alternative approaches may suggest an uncertainty in topographic data or the employed approach. In the meantime, this threshold keeps a sufficient number of catchments to ensure the subsequent statistical study had a meaningful sample size.

This filtering procedure left us with 1033 catchments in the United States and Canada with areas ranging from 50 to 273 000 km<sup>2</sup> (Figure 1).

### 2.2 | Climate attributes

Climate attributes used in our study were obtained from the ERA5-Land (ERA5-L) database (Muñoz-Sabater et al., 2021) for the period between 1981 and 2019. ERA5-L assimilates different sources of climate data to estimate global climate on land masses at 9 km<sup>2</sup> spatial resolution at both hourly and monthly time resolutions. Here, the hourly data extracted from the database includes: temperature, total precipitation, rainfall, snowmelt, and snow depth, along with monthly total precipitation, snow density and actual (and potential) evapotranspiration. We acknowledge that some of these attributes, including snowmelt and actual evapotranspiration, are modelled output and are prone to uncertainty. Particularly, the snowmelt data were not sufficiently validated against field data and are therefore inherently more uncertain.

Using this data, we calculated seven process-oriented climatic attributes, including long-term (1981–2019) average annual water surplus, long-term average water input intensity, seasonality index, snow fraction, aridity index, long-term average annual maximum snow water equivalent, and long-term average day of annual maximum snow depth (Table 1). The long-term average annual water surplus is calculated as the average of the sum of differences between monthly rainfall/snowmelt and actual evapotranspiration in each year. Long-term average water input intensity is the average of daily water input intensity over 1981–2019, where daily water input intensity was calculated as the sum of rainfall and snowmelt in those water input events exceeding 1 mm/day threshold. Adopting the method suggested by Woods (2009), we calculated seasonality index based on the implicit interaction between

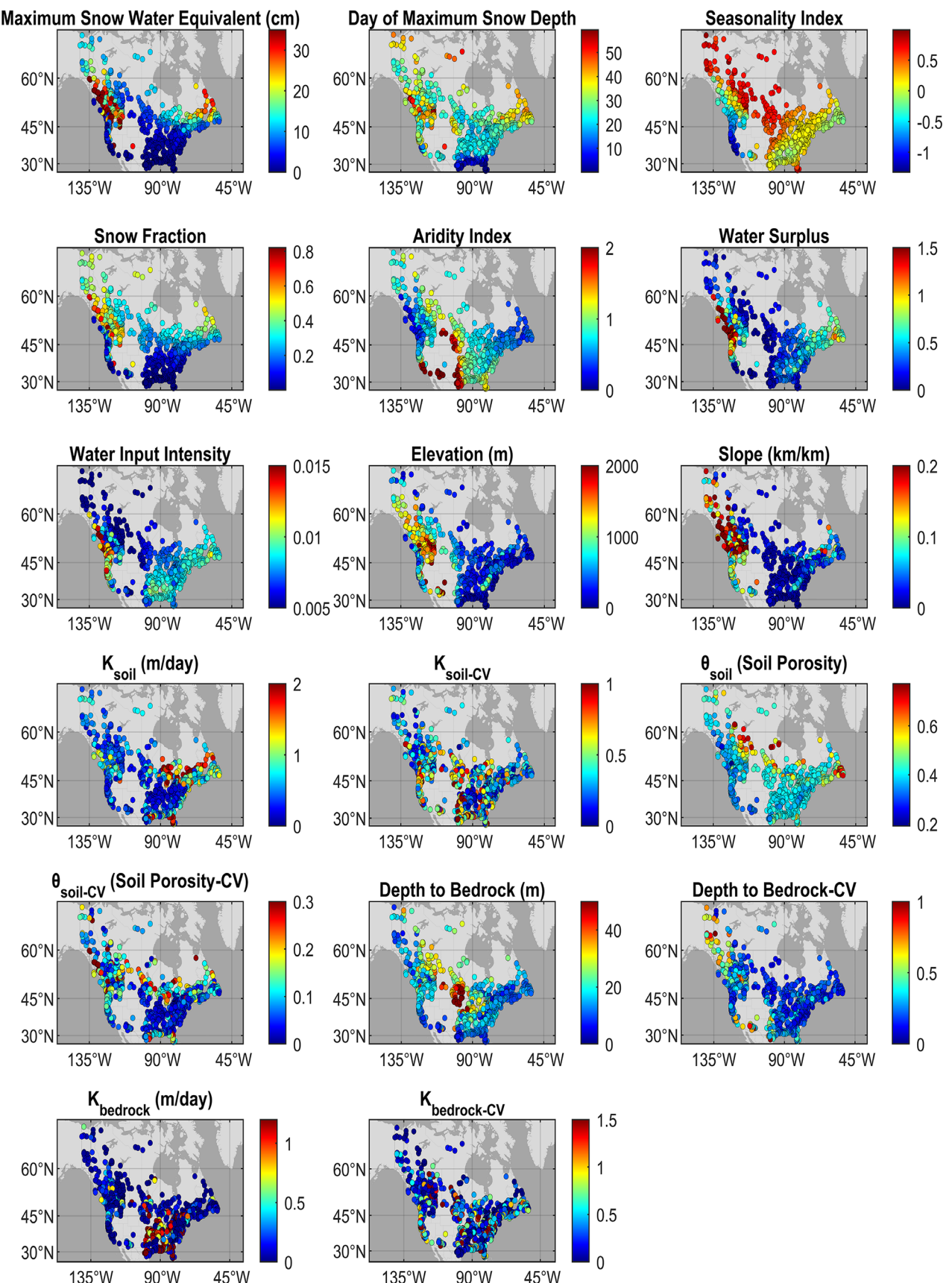


**FIGURE 1** Overview of catchment locations and catchment-scale climatic, topographical and geological attributes. The median and interquartile ranges of attributes, across the study area, are reported in Table 1. CV for a given attribute stands for catchment-scale coefficient of variation of the attribute: The ratio of the horizontal within catchment standard deviation ( $SD$ ) of the attribute to catchment-scale average value of the attribute. The unit of day of maximum snow depth is day number from the first day of February.

hourly precipitation and temperature. We calculated snow fraction as the ratio between long-term average annual snowmelt to annual total precipitation, and aridity index as the ratio between long-term average annual potential evapotranspiration to annual total precipitation. Annual maximum snow depth was calculated as the maximum snow depth daily value within the period between the first day of February and the first day of May in each year, using daily snow depth data. Similarly, the long-term average day of annual maximum snow depth was calculated as the average of the day of maximum snow depth in each year, over 1981–2019. The long-term average annual maximum snow water equivalent was calculated as the average of the annual maximum snow water equivalent for each year. Annual maximum snow water equivalent for each year (SWE) (cm) is given by:

$$\text{SWE} = h_s \left( \frac{\rho_s}{\rho_w} \right) \quad (2)$$

where  $h_s$  is the annual maximum snow depth (cm) for each year,  $\rho_s$  is snow density at the day of maximum snow depth ( $\text{g cm}^{-3}$ ) and  $\rho_w$  is density of water ( $1 \text{ g cm}^{-3}$ ).

**TABLE 1** Description of catchment-scale physical and climatic attributes.

	Attributes	Unit	Median (Q1–Q3)	Feature importance	Prediction
Climatic	Maximum snow water equivalent	cm	6.64 (1.89–16.0)	▲	●
	Day of maximum snow depth	day	25.54 (21.43–33.65)	▲	●
	Seasonality index <sup>a</sup>	—	0.11 (−0.06–0.29)	▲ <sup>a</sup>	●
	Snow fraction <sup>b</sup>	—	0.22 (0.07–0.34)	▲ <sup>b</sup>	●
	Aridity index	—	0.71 (0.50–0.94)	▲	●
	Water surplus	m	0.40 (0.24–0.65)	▲	●
	Water input intensity	m/day	0.008 (0.007–0.009)	▲	●
Topographic	Area	$\text{km}^2$	478.70 (203.66–1444.37)	●	●
	Elevation	m	394.81 (231.03–824.15)	●	●
	Slope	km/km	0.04 (0.01–0.09)	▲	●
	Longitude	—	88.53 (78.10–117.13)	●	●
Physical	$K_{\text{soil}}$	m/day	0.47 (0.28–0.82)	▲	●
	$K_{\text{soil-CV}}$	—	0.32 (0.20–0.55)	▲	●
	$\theta_{\text{soil}}$ (soil porosity)	—	0.40 (0.37–0.45)	▲	●
	$\theta_{\text{soil-CV}}$ (soil porosity-CV)	—	0.07 (0.04–0.12)	▲	●
	Depth to bedrock	m	15.17 (11.22–21.30)	▲	●
	Depth to bedrock-CV	—	0.20 (0.15–0.29)	▲	●
	$K_{\text{bedrock}}$	m/day	0.08 (0.01–0.31)	▲	●
	$K_{\text{bedrock-CV}}$	—	0.23 (0.05–0.55)	▲	●

Note: Median and interquartile ranges of the attributes, over all catchments, are reported. CV for a given attribute stands for catchment-scale coefficient of variation of the attribute: The ratio of the horizontal within catchment SD of the attribute to catchment-scale average of the attribute. The last two columns indicate whether a given attribute was used in the feature importance analysis (see Section 3.2) or in the prediction in gauged to poorly-gauged regions (see Section 3.3).

<sup>a</sup>Seasonality index was only used for feature importance analysis of medium size catchments and was not among the attributes used in the feature importance analysis of the large catchments.

<sup>b</sup>Snow fraction was only used for feature importance analysis of large catchments and was not among the attributes used in the feature importance analysis of the medium size catchments.

### 2.3 | Catchment physical attributes

A total of 12 topographical, soil, and geological attributes used in our study are as follows (and Table 1). Note that the average catchment-scale value of a given attribute was calculated as the average of the attribute's values of all cells within the catchment boundary polygon. Catchment-scale coefficient of variation (CV) of a given attribute was calculated as the ratio between the standard deviation (SD) of the attribute values of all grid cells within the catchment boundary polygon to the average catchment-scale value of the attribute. The coefficient of variation of an attribute reflects the horizontal variation of grid cells' values of the given attribute within the catchment's boundary polygon.

- Slope: average catchment-scale slope.
- Elevation: average catchment-scale elevation.
- Area: area within the catchment's boundary polygon.
- Longitude: average catchment-scale longitude.
- $K_{\text{soil}}$ : average catchment-scale soil saturated hydraulic conductivity.
- $K_{\text{soil-CV}}$ : catchment-scale coefficient of variation of  $K_{\text{soil}}$ .
- $\theta_{\text{soil}}$ : average catchment-scale soil porosity.

- $\theta_{\text{soil-CV}}$ : catchment-scale coefficient of variation of soil porosity.
- Depth to bedrock: average catchment-scale depth to bedrock.
- Depth to bedrock-CV: catchment-scale coefficient of variation of depth to bedrock.
- $K_{\text{bedrock}}$ : average catchment-scale bedrock hydraulic conductivity.
- $K_{\text{bedrock-CV}}$ : catchment-scale coefficient of variation of bedrock hydraulic conductivity.

### 2.3.1 | Topographical attributes

Elevation, flow direction and flow accumulation data were retrieved from 90-m resolution MERIT Hydro database (Yamazaki et al., 2019) in order to derive catchment boundary polygons for Canadian gauges using the Watershed Tool in ArcGIS with D8 flow modelling algorithm. Average catchment slope, elevation and longitude were then calculated using boundary polygons of Canadian catchments along with readily available polygons for the CAMELS catchments in the United States. One other potential topographical attribute that could control recession parameters is drainage length as suggested in hydraulic groundwater theory (e.g., Marçais et al., 2017; Troch et al., 2003). However, our preliminary results showed that this parameter is not among the 15 top-ranked attributes that control recession parameters for both medium size and large catchments. Therefore, this parameter was not included in our final analyses.

### 2.3.2 | Soil attributes

The soil hydraulic properties, including porosity, hydraulic conductivity and depth to bedrock, were extracted from a gridded (900-m<sup>2</sup> resolution) global-scale database developed by Dai et al. (2019) and Shangguan et al. (2017). Note that depth to bedrock includes soil and unconsolidated deposits.

### 2.3.3 | Geological attributes

Bedrock hydraulic conductivities of catchments were calculated based on global-scale bedrock permeability developed by Huscroft et al. (2018). We also used the equation suggested by Gleeson et al. (2014) to convert bedrock permeability to bedrock hydraulic conductivity.

## 3 | METHODS

### 3.1 | Recession analysis

While many previous studies have investigated recession parameters by fitting an equation to the log-log plot of the all-time streamflow versus its time derivative “point cloud” (e.g., Brutsaert & Nieber, 1977; Kirchner, 2009; Vogel & Kroll, 1992), current literature suggests deriving recession parameters using each individual

recession event (e.g., Basso et al., 2015; Biswal & Marani, 2010; Chen & Krajewski, 2016; Dralle et al., 2017; Jachens et al., 2020; Karlsen et al., 2019; Roques et al., 2017; Shaw & Riha, 2012; Tashie et al., 2020b). The advantage of individual recession event analysis is that both seasonal and annual trends in the recession behaviour become available by determining  $a$  and  $b$  values for each individual event. It is also noted repeatedly in the literature that  $b$  values obtained from individual events are generally greater than typical values calculated from point cloud, more realistically representing high nonlinearities in early-stage recession and late-stage recession (Ghosh et al., 2016; Jachens et al., 2020; Mutzner et al., 2013; Roques et al., 2017; Tashie et al., 2019; Tashie et al., 2020a; Tashie et al., 2020b). The derivation of recession parameters in our study relies on the individual recession event method to account for catchment behaviours in both early-stage and late-stage recession, and these results are then used in subsequent analyses. Here, we adopted Tashie et al. (2020b) filtering criteria to identify recession events, where both streamflow and its negative time derivative ( $-dQ/dt$ ) must monotonically decrease for at least five consecutive days. The first day of recession was removed to minimize the influence of overland flow. We identified 106 170 recession events in 1033 studied catchments. The number of recession events identified in each catchment ranged from 26 to 430.

The recession parameters were determined for each unique recession event using linear regression on the log transformed plane of  $-dQ/dt$  versus  $Q$ . The former (i.e., the time derivative of discharge) was calculated using forward finite difference estimation, one of the constant time step methods. The slope obtained from linear regression in each event refers to the recession nonlinearity ( $b$ ) for that event (Figure 2a). For each catchment, the median value of recession nonlinearity across all eligible events was then used as the catchment's representative  $b$  value (Figure 2a). To calculate  $\log(a)$  (or  $y$ -intercept) for each event, we ran a linear regression for each event again, but this time using a fixed constant slope. Here, a fixed constant slope of 2.86 was considered for all catchments, which represents the median value of all catchments' representative  $b$  values determined in the previous step (as will be shown in section 4.1.2). This approach avoids the reported covariation of  $\log(a)$  with  $b$  and enables us to fairly compare  $\log(a)$  values among events and catchments without the confounding effect of  $b$ . For a given catchment, once  $\log(a)$  for each event was calculated, the median value of  $\log(a)$  of all events in the catchment was the catchment's representative  $\log(a)$  or recession instability (Figure 2b). Additionally, a fixed constant slope of 1.5 was considered to calculate a catchment's representative  $\log(a)$  and to explore the sensitivity of  $\log(a)$  spatial pattern and drivers to the fixed value of parameter  $b$ . Figures corresponding to a fixed slope of 1.5 are shown in the supplementary document. Note that  $b = 2.86$  is close to the suggested recession nonlinearity by hydraulic groundwater theory (i.e.,  $b = 3$ ) for infinitely long horizontal aquifer with a fully saturated initial condition.  $b = 1.5$  was also suggested by hydraulic groundwater theory as the recession nonlinearity of an infinitely long horizontal aquifer with inverse beta function as an initial condition (Huyck et al., 2005).

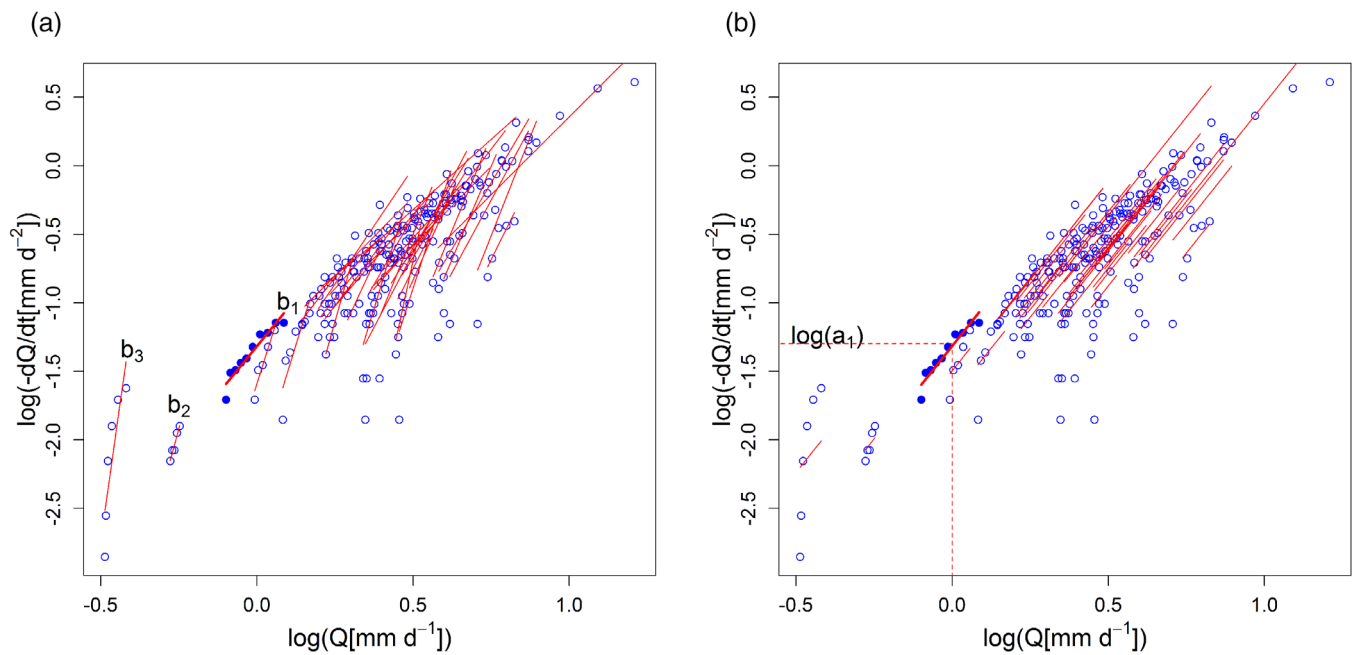


**FIGURE 2** Recession analyses plots in log-log space for Fantail River at outlet of Fantail Lake (Yukon, Canada; ID 09AA014). Blue circles refer to logarithmic streamflow time derivatives plotted against logarithmic streamflow. Red lines are linear regression fit for each recession event. (a) Linear regression of individual recession events where  $b_i$  denotes the slope of linear fit for  $i$ th recession event. (b) Linear regression of individual recession events with a fixed slope of 2.86 (median of all catchments'  $b$  values) to determine  $y$ -intercept or  $\log(a_i)$  for each event. Event No. 1 is highlighted with filled blue circles and thick red line in both panels.

### 3.2 | Marginal contribution feature (attribute) importance with random forests

We used catchments' physical and climatic attributes as explanatory variables, and catchments'  $\log(a)$  and  $b$  values as two response variables, in a random forests framework, to identify the importance of catchments' attributes in explaining the hydrograph recession parameters.

Identifying the importance of catchments' attributes in explaining streamflow signatures is now a common practice to determine the drivers of streamflow generation mechanisms. Previous regional studies, focused on identifying the dominant drivers of streamflow, are sometimes using linear models or statistical approaches that are negatively impacted by collinearities—and/or do not deal with the interactions—among a catchment's attributes (e.g., Mutzner et al., 2013; Tashie et al., 2020b; Ye et al., 2014). For example, the approach of identifying the importance of an attribute as the increase in mean square error in a random forests model by shuffling that attribute, as done in Addor et al. (2018) (among others), may not sufficiently estimate the importance of some attributes (e.g., soil conductivity & depth to bedrock) due to their high correlation with other dominant (e.g., climatic, topographic) attributes. Hydrologic datasets usually contain several correlated attributes (Figure 3) due to the coevolution among catchment attributes (Blöschl et al., 2014). Furthermore, the interaction among climatic, geological and topographical attributes in explaining streamflow generation mechanisms were shown using

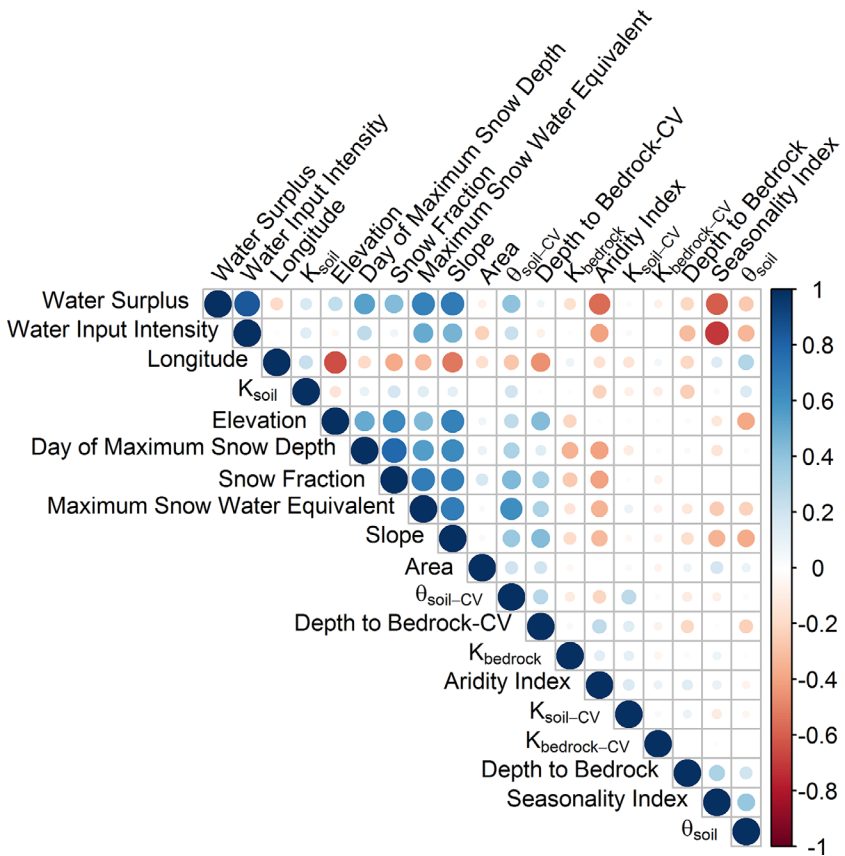
experimental, empirical and theoretical studies (Janssen & Ameli, 2021), which were not thoroughly considered in some previous feature importance studies (e.g., Juhn et al., 2020).

Here, we coupled random forests with the marginal contribution feature importance (MCI) approach developed by Catav et al. (2020):

$$I_v(f) = \max_{S \subseteq F} \Delta(f, S, v) \quad (3)$$

where  $I_v(f)$  is the importance of feature  $f$ ,  $S$  denotes any subset of features from the power set of  $F$  that includes all features, and  $v$  is the evaluation function monitoring the model gain/loss.  $\Delta(f, S, v) = v(S \cup \{f\}) - v(f)$  denotes the reduction in evaluation function when removing the feature  $f$ . Like other feature importance algorithms used with random forests before, MCI function computes the gain/loss of model performance when adding/eliminating each attribute in order to rank the attributes' importance. In doing so, however, MCI function uniquely contains marginal contribution, elimination and minimalism. These mean that, (1) the importance of a feature is at least as large as the decrease in loss when adding the feature, (2) eliminating the feature in each iteration can only decrease the other features' importance, and (3) the feature importance score is the smallest value that satisfies the previous two constraints. To ensure the robustness against the correlated/duplicated attributes, MCI employs a duplication invariance property, which means that when information among features are duplicated the features importance scores do not change. Furthermore, the random forests portion of our coupled

**FIGURE 3** Pearson correlation ( $r$ ) among attributes.



feature importance algorithm could consider a wide range of interactions among attributes as discussed in Luo et al. (2018).

We computed the MCI function for  $2^{15}$  (15 = total number of features) randomly sampled subsets of the power set of  $F$  (i.e., 32768 sets made of combinations of 15 features). Note that due to a high computational cost of MCI, we had to limit the number of evaluated attributes to 15 in each feature importance analysis. In identifying the feature (attribute) importance, we divided the 1033 catchments into three groups:

- A total of 391, medium size ( $50\text{--}1000 \text{ km}^2$ ) rain-dominated catchments (snow fraction  $<20\%$ )
- A total of 310, medium size snow-dominated catchments (snow fraction  $>20\%$ )
- A total of 332, large size catchments ( $\text{area } >1000 \text{ km}^2$ )

A snow fraction threshold of 20% was used to divide catchments between rain versus snow dominated following the characterization made by Davenport et al. (2020). An aerial threshold of  $1000 \text{ km}^2$  was used to divide catchments between medium size and large size. This threshold was adopted from Wu et al. (2021) and could to some extent consider the large effect of time delay on streamflow recession in large catchments.

For two groups of medium size catchments, we applied the MCI function to 15 explanatory climate, geologic and topographical attributes including: aridity index, water surplus, water input intensity,

maximum snow water equivalent, day of maximum snow depth, seasonality index,  $K_{\text{soil}}$ ,  $K_{\text{soil}}\text{-CV}$ ,  $\theta_{\text{soil}}$ ,  $\theta_{\text{soil}}\text{-CV}$ , depth to bedrock, depth to bedrock-CV,  $K_{\text{bedrock}}$ ,  $K_{\text{bedrock}}\text{-CV}$ , and slope (Table 1), against two response variables  $\log(a)$  and  $b$ . Snow fraction was not among explanatory attributes as we divided the medium size catchments based on their snow fractions. For large size catchments, we added snow fraction into the random forests, but removed seasonality index, as the preliminary experiments showed that seasonality index has overall less importance than any other climatic attributes in large catchments. Our preliminary analyses also showed that drainage length was not among top-ranked 15 attributes that control recession parameters for both medium and large size catchments.

### 3.3 | Random forests predictions of streamflow recession parameters in gauged to poorly-gauged regions

To test the predictive power of random forests we added three additional explanatory variables, including elevation, longitude, and area, to the list of explanatory attributes used in the feature importance tests (Table 1; last column). These attributes were excluded in the feature importance tests due to their small importance identified in the preliminary analyses of three considered groups, and because our feature importance method's limit on the number of attributes that can be considered. However, they can still slightly

improve the overall predictive capability of random forests models, as they may indirectly reflect the contributions of other variables which were not included in our study. For each recession parameter, we developed a predictive model using all 1033 catchments, without grouping the catchments based on their size or snow fraction.

We chose four different cross validation algorithms with random forests, wherein the portion of samples used to train versus test the model varies among algorithms. In the first algorithm, the random forests model was trained on the entire dataset (i.e., 1033 catchments) to simulate recession parameters, and then the trained models were tested on the same dataset used for training. This algorithm roughly emulates a hypothetical scenario of random forests predicting recession parameters in extensively gauged regions. In the second cross validation algorithm, a leave one out cross-validation criterion was used, by predicting a catchment's recession parameters from trees in the trained random forests model that did not use the catchment of interest in training, then iterating through each catchment. This algorithm roughly emulates a hypothetical scenario of random forests predicting recession parameters in semi-gauged regions (Semi-gauged 1). In the third algorithm, five-fold-cross-validation was conducted by randomly splitting the 1033 catchments into five “folds”, then iteratively training on the four folds (80% of catchments) and testing on the remaining fold (20% of catchments). Again, this algorithm roughly emulates a hypothetical scenario of random forests predicting recession parameters in semi-gauged regions (Semi-gauged 2). In the fourth algorithm, multiple predicting five-fold cross-validation (MPCV) (Jung, 2018) was used. In this algorithm we randomly divided the dataset into five folds, then iteratively training on one-fold (20% of catchments), and testing on the remaining four folds (80% of catchments). Basically, MPCV could roughly emulate a hypothetical scenario of random forests predicting recession parameters in poorly-gauged regions (poorly gauged). Collectively, four different cross-validation algorithms compare the random forests predictive capabilities across a hypothetical spectrum of gauged to poorly-gauged regions.

The performance of all four algorithms were measured with the generalized coefficient of determination  $R^2$ :

$$R^2 = 1 - \frac{\sum_{i=1}^n (\hat{y}_i - y_i)^2}{\sum_{i=1}^n (y_i - \bar{y})^2} \quad (4)$$

For each cross-validation algorithm,  $\hat{y}$  is the simulated recession parameter (recession instability or nonlinearity) in the validation phase, while  $y$  (and  $\bar{y}$ ) refers to the recession parameter values (and their averages) estimated using hydrograph recession analysis.  $n$  represents the number of samples (catchments) used in the testing phase. Since random forests and creating the folds are stochastic, we replicated each experiment 200 times and recorded the mean and standard deviation ( $SD$ ) of  $R^2$  values. A smaller  $SD$  shows the stability of  $R^2$  across the random experimentations.

## 4 | RESULTS

In this section, we first show the spatial patterns of recession parameters (Section 4.1). Then we report the results of feature (attribute) importance for recession instability (Section 4.2) and nonlinearity (Section 4.3), in rain-dominated versus snow-dominated catchments as well as in medium versus large size catchments. In Section 4.4, we show the random forests predictive capabilities of streamflow recession parameters in gauged to poorly-gauged regions.

### 4.1 | Recession analysis

#### 4.1.1 | Spatial pattern of recession instability ( $\log[a]$ )

Recession instability  $\log(a)$  has a median of  $-1.04$  and ranged from  $-3.68$  to  $5.87$  across our studied catchments. Here a larger  $\log(a)$  shows a higher recession instability, or a lower recession stability. The central United States and Canada, generally, exhibits higher recession instability than Eastern and Western portions (Figure 4 for  $b = 2.86$ , Figure S2 for  $b = 1.5$ ). In the Western portion of our study area recession instability generally increases from north to south.

#### 4.1.2 | Spatial pattern of recession nonlinearity

The values of recession nonlinearity,  $b$ , are between 2 and 4 for 72% (743 out of 1033) of the catchments. Nonlinearity  $b$  values range from a minimum of  $1.09$  to a maximum of  $15.55$  with a median of  $2.86$ . Compared with the visible spatial pattern of  $\log(a)$ , the spatial pattern of  $b$  is less obvious except consistently large nonlinearities estimated across the Rocky Mountain catchments (Figure 5). Figure S1 shows the histograms of  $b$  values for three groups of catchments analysed in our paper. The histogram, generally, does not show a distinct distribution of  $b$  among three groups. The medians of medium size rain-dominated, medium size snow-dominated, and large size catchments are  $2.52$ ,  $3.03$  and  $3.25$ , respectively.

### 4.2 | What factors affect recession (in)stability?

In all catchment groups, climatic attributes showed greater influence on recession (in)stability than slope and soil/geological attributes (Figure 6 for  $b = 2.86$ , Figure S3 for  $b = 1.5$ ). The relative importance of climatic attributes (blue colour), compared to physical attributes (red and green), is larger in snow-dominated catchments (Figure 6b) and in large catchments (Figure 6c) than in medium size rain-dominated catchments. In rain-dominated medium size catchments, among belowground attributes, slope and depth to bedrock coefficient of variation were among moderately important attributes (relative importance score between 0.5 and 0.75). In snow-dominated medium size catchments, however, only one belowground attribute,

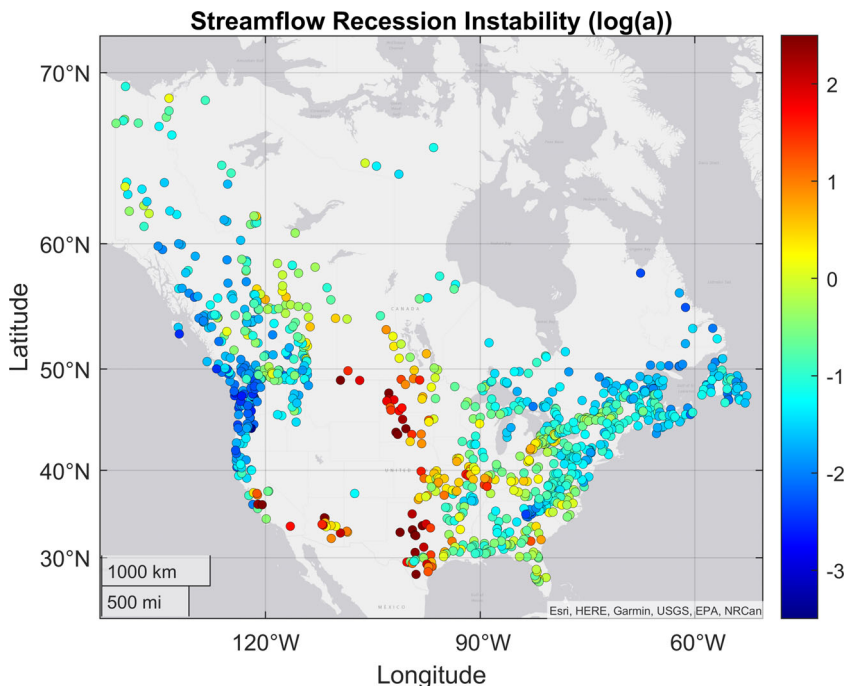


**FIGURE 4** Recession instability for 1033 catchments in the United States and Canada. A larger  $\log(a)$  shows a higher recession instability. Red colour refers to less stable streamflow, and blue colour refers to more stable streamflow. This figure shows  $\log(a)$  spatial pattern obtained using a fixed constant slope of 2.86. Figure S2 (supplementary material) shows the  $\log(a)$  spatial pattern obtained using a fixed constant slope of 1.5.

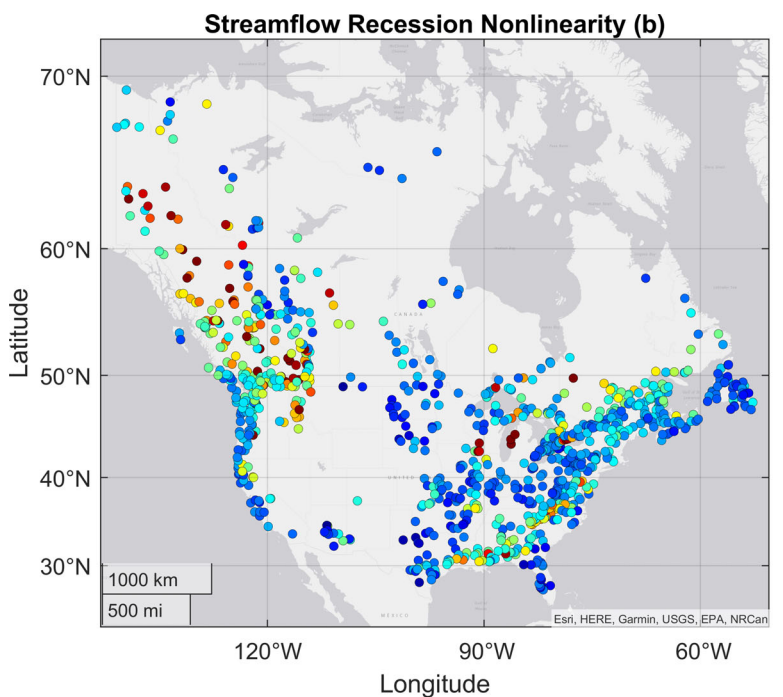


**FIGURE 5** Streamflow recession nonlinearity (b) for 1033 catchments in the United States and Canada. Red colour refers to more nonlinear streamflow recession, and blue refers to more linear streamflow recession.

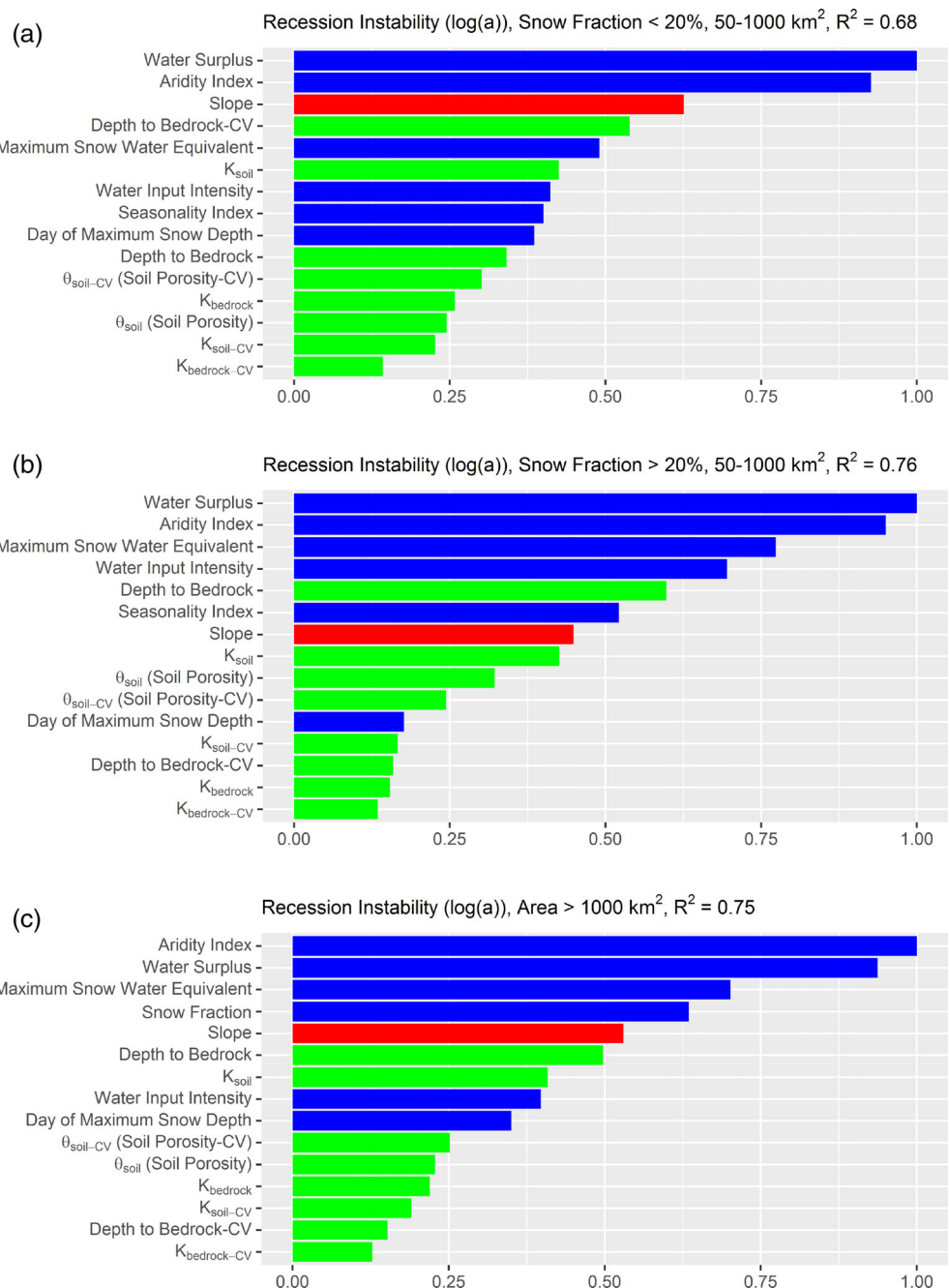
depth to bedrock, was among moderately important attributes. None of the soil or bedrock attributes' relative scores were over 0.5 in large size catchment group. Water surplus and aridity index are the dominant factors (relative importance score  $>0.75$ ) in rain-dominated medium size catchments, while water surplus, aridity index and maximum snow water equivalent are the dominant driving factors in snow-dominated medium size catchments. In large catchments, aridity index and water surplus become relatively the dominant drivers of recession (in)stability followed by maximum snow water equivalent.

These conclusions are consistent between  $\log(a)$  values calculated using a fixed constant slope of 2.86 (Figure 6) and  $\log(a)$  values calculated using a fixed constant slope of 1.5 (Figure S3).

#### 4.3 | What factors affect recession nonlinearity?

Physical attributes are relatively more influential for nonlinearity  $b$  (Figure 7) than for instability  $\log(a)$ , especially in the rain-dominated

**FIGURE 6** Feature importance scores and rankings for recession instability  $\log(a)$  for (a) Medium size rain-dominated catchments; (b) Medium size snow-dominated catchments; (c) Large size catchments. Here,  $R^2$  values refer to the 5-fold cross-validation  $R^2$  of random forest. The feature importance scores are normalized for each catchment group with respect to the largest importance score within the group, in a manner similar to Stein et al. (2021). This allows the assessment of the differences in attributes' rankings between three groups with distinct dominant precipitation type or distinct scale. Colours refer to different attribute categories: Blue for climate, green for soil and bedrock, and red for topography. This figure shows feature importance scores for  $\log(a)$  calculated using a fixed constant slope of 2.86. Figure S3 (supplementary material) shows feature importance scores for  $\log(a)$  obtained using a fixed constant slope of 1.5.



medium size group. Soil porosity ( $\theta_{\text{soil}}$ ),  $K_{\text{bedrock}}$ , depth to bedrock and  $K_{\text{soil}}$  are the four belowground attributes with a normalized score of over 0.75 for recession nonlinearity in rain-dominated medium size catchments (Figure 7a). However, the relative importance of these below-ground attributes slightly drops in snow-dominated medium size catchments (Figure 7b) and significantly drops in large size catchments (Figure 7c). In medium size snow-dominated and large size catchments, slope becomes the dominant attribute driving the nonlinearity  $b$  followed by maximum snow water equivalent. Slope is also among most important drivers of nonlinearity  $b$  in the rain-dominated medium size group.

#### 4.4 | Random forests prediction of recession parameters in gauged to poorly-gauged regions

The capabilities of random forests are stronger in predicting recession instability  $\log(a)$  than nonlinearity  $b$  (Figure 8). The cross-validation  $R^2$  values for predicting  $\log(a)$  are 0.96, 0.80, 0.79, and 0.71 in four cross validation algorithms spanning the predictions in gauged to poorly-gauged regions. Meanwhile, the  $R^2$  values for nonlinearity  $b$  in four cross validation algorithms are 0.91, 0.50, 0.49, and 0.40.

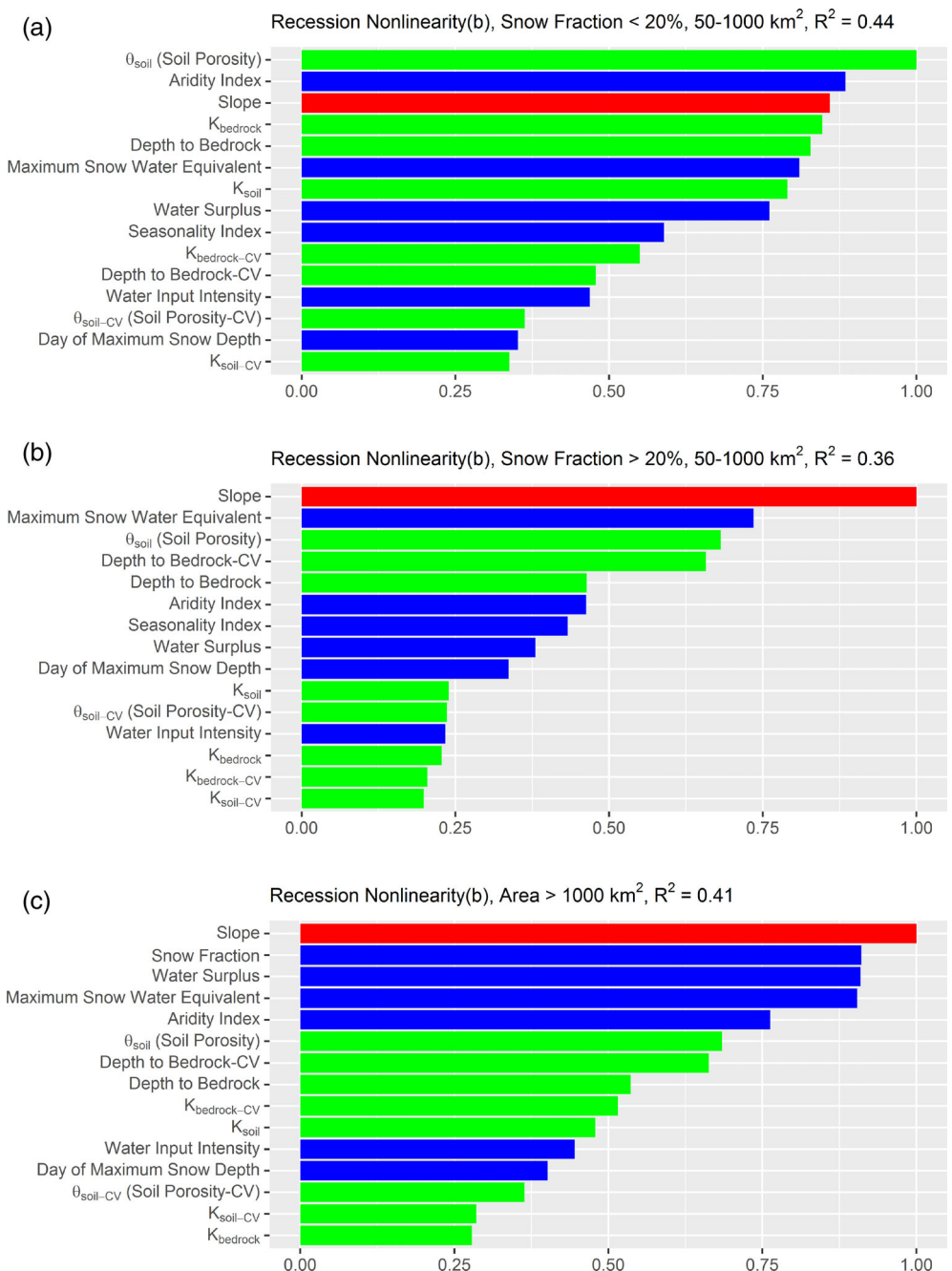


**FIGURE 7** Feature importance scores and rankings for recession nonlinearity  $b$  in, (a) Medium size rain-dominated catchments; (b) Medium size snow-dominated catchments; (c) Large size catchments. Here,  $R^2$  values refer to the 5-fold cross-validation  $R^2$  of random forest. The feature importance scores are normalized for each catchment group with respect to the largest importance score within that group. Colours refer to different attribute categories: Blue for climate, green for soil and bedrock, and red for topography.

## 5 | DISCUSSION

### 5.1 | Spatial distribution of recession parameters

Our findings highlight that streamflow recession is more stable or subsurface storage capacity is higher ( $\log(a)$  is smaller) in coastal climate zones than in continental climate zones, consistent with the results presented by Tashie et al. (2020b). This trend can be explained by the relatively large influence of climatic attributes on  $\log(a)$  (Figure 6). Indeed, the spatial variations of climatic attributes (Figure 1) may reflect the spatial variations of recession (in)stability (Figure 4). The spatial variations of climatic attributes are distributed coastal to continental for aridity index, water surplus, and water input intensity

(Figure 1). Meanwhile, catchments in southwest United States tend to have a slightly less stable recession ( $\log(a)$  is larger) than those in Pacific northwest, so is it true for catchments in southeast United States to generally have less stable recession than those in northeast United States and eastern Canada.

Recession nonlinearity ( $b$ ), however, has a less obvious spatial pattern, which again coincides with the findings revealed by Tashie et al. (2020b), except along the Rocky Mountains (in both Canada and the United States) where recession nonlinearities are consistently high. Our results depict less importance of the catchment climate attributes and more importance of the physical attributes including soil properties and slope (Figure 7). Soil properties and slope generally do not display spatial patterns as clear as climatic attributes (Figure 1). The

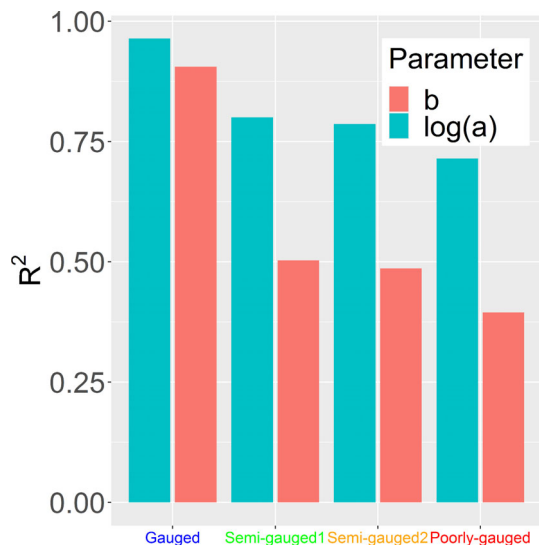


**FIGURE 8** Cross-validation  $R^2$  values for random forests prediction of recession parameters using four cross validation algorithms, spanning the predictions in gauged to poorly-gauged regions. The reported  $R^2$  values are the averages of 200 iterations in each cross-validation algorithm. The SDs of the  $R^2$ , across the 200 iterations, for the prediction of  $\log(a)$  were 0.0006, 0.002, 0.005 and 0.006, along four cross-validation algorithm. The SDs of the  $R^2$  for the prediction of  $b$  were 0.001, 0.004, 0.01 and 0.007.

lack of spatial pattern in recession nonlinearity can be attributed to the lack of spatial patterns in soil and topographical attributes, which strongly control recession nonlinearity. One possible explanation for the consistently high nonlinearity values along the Rocky Mountain catchments is that slope and maximum snow water equivalent, as the dominant factors of recession nonlinearity in snow-dominated catchments (Figure 7b), are consistently large at these sites (Figure 1).

## 5.2 | Do the drivers of recession behaviour differ between rain-dominated and snow-dominated medium size catchments?

For recession (in)stability, the relative importance of belowground attributes are all lower in snow-dominated compared to rain-dominated catchments (Figure 6). Alternately, maximum snow water equivalent is among the dominant drivers of recession (in)stability in snow-dominated catchments. These points together may suggest that in snow-dominated catchments, in comparison to rain-dominated catchments, snowmelt impacts on subsurface storage and recession (in)stability are relatively less dependent on catchment belowground attributes, but relatively more dependent on how much water the largest snowmelt events could create.

The average slope is among the most important drivers of recession nonlinearity ( $b$ ) in both snow-dominated and rain-dominated catchments (Figure 7), as suggested by previous theoretical analyses (e.g., Rupp & Selker, 2006). The dominancy of slope on recession nonlinearity could be attributed to slope's controls on catchment

hydrologic functions, defined as the ways catchments partition, store and release input water. All three functions impact recession nonlinearity (Brutsaert, 2005; Troch et al., 2013). At the sametime, slope could directly control storage, partitioning and release functions (Janssen & Ameli, 2021; Li et al., 2014).

The relative influences of belowground attributes on recession nonlinearity ( $b$ ) are much larger in rain-dominated catchments than snow-dominated catchments (Figure 7a,b), while maximum snow water equivalent dominantly controls recession nonlinearity in snow-dominated catchments. Indeed, the nonlinearity of recession in snow-dominated catchments depends on how snow accumulates and when (and how fast) it melts. On the other hand, in rain-dominated catchments, the contribution of rainfall events to recession nonlinearity highly depends on how belowground attributes filters and transfers input rainfall to streamflow. In rain-dominated catchments, the formation of hydrologic connectivity along the soil-bedrock interface is strongly controlled by belowground attributes. Previous research showed that the formation of hydrologic connectivity along the soil-bedrock interface is the main streamflow generation mechanism in several rain-dominated forested catchments (as shown in Ameli et al., 2015; Hopp & McDonnell, 2009). These points together may explain larger influences of catchment soil/geological attributes on recession nonlinearity in rain-dominated catchments.

Generally, our statistical large sample hydrology analyses suggest that streamflow recession behaviour and subsurface storage-release processes depend on belowground attributes and slope in rain-dominated medium size catchments, and depend on slope and how snow accumulates and when it melts in snow-dominated medium size catchments. Furthermore, the dominancy of maximum snow water equivalent on recession parameters in snow-dominated medium size catchments (Figures 6 and 7) could be important in the light of climate change. This attribute is highly vulnerable to the reductions in snow fraction and snow depth as well as earlier snowmelt (e.g., Musselman et al., 2017) which may occur with changing climate. This suggests that climate change could alter storage-release processes in snow-dominated catchments through alterations in maximum snow water equivalent. Additionally, the above findings emphasize the distinct drivers of storage-release processes in rain versus snow dominated catchments. This implies that an alteration in storage-release processes could be expected if climate change varies dominant precipitation type in a given catchment or varies dominant climatic drivers of rain-dominated or snow-dominated catchments (e.g., aridity index, maximum snow water equivalent).

## 5.3 | The effects of spatial heterogeneity of catchments' physical attributes on recession instability and nonlinearity

The coefficient of variations of belowground attributes do not generally show a significant influence on recession instability or nonlinearity. The only two exceptions are the coefficient of variation for depth to bedrock in the rain-dominated medium size group for explaining

$\log(a)$  and in the snow-dominated medium size group for explaining  $b$ . Low relative importance of the coefficient of variations for physical attributes, obtained in our analyses, may not suggest that spatial heterogeneities of physical attributes are not influential on catchment-scale recession parameters. Rather, it could be due to the fact that the coefficient of variations of physical attributes are merely a rough representation of catchment spatial hydraulic heterogeneity and therefore cannot sufficiently reflect the accurate influence of lateral heterogeneity on streamflow recession. Furthermore, while the databases on soil and bedrock properties we used in our paper are clearly an important contribution, they are drawn from sparse local borehole data extrapolated according to the lithology. This means that they might not capture “true” lateral heterogeneities of subsurface properties.

#### 5.4 | Does catchment size differentiate the primary drivers of streamflow recession behaviours?

As catchment size increases, the relative importance of climatic attributes on both recession parameters generally increases, while the relative importance of soil and bedrock hydraulics are all dropped (Figures 6 and 7). Indeed, the streamflow recession behaviour and storage-release processes of a medium size catchment can be very sensitive to catchment belowground attributes, while in a large catchment the attributes related to magnitude and timing of input water (e.g., water surplus, aridity index, snow water equivalent) dictates streamflow recession behaviour. Furthermore, our results show that the recession nonlinearity generally enhances with an increase in catchment size (Figure S1). This finding corroborates with the experimental study conducted by Clark et al. (2009) and theoretical analysis conducted by Harman et al. (2009) and Ranjram and Craig (2021).

#### 5.5 | Limitation of the study and future research

To test the importance of within-catchment lateral heterogeneities of physical attributes, we employed the coefficient of variation of soil and bedrock attributes. This provides insightful information on processes controlling streamflow recession behaviours that cannot otherwise be obtained by using catchment average physical attributes alone. However, the coefficient of variation of (most) catchment physical attributes is not sufficient to fully describe the complicated spatial heterogeneities of these attributes. The actual impact of these heterogeneities might be larger than what our study has suggested. Furthermore, in the experiment of predicting recession parameters in gauged to poorly-gauged regions (Section 4.4), random forests models predicted  $\log(a)$  with a relatively high accuracy, while  $b$  was not very well predicted. This difference is likely due to the spatial heterogeneities of catchments' physical attributes which could have controlled  $b$  but are not well incorporated in our analyses. These heterogeneities, that occur at a small spatial scales, may not be well quantified in the available databases as they are drawn from sparse observations. Higher

resolution field data of physical attributes are crucial for further improving the analysis and prediction of recession parameters.

In estimating recession parameters (Section 3.1), we used a constant time step forward finite difference method to estimate the time derivative of streamflow. As suggested by Roques et al. (2017) and Thomas et al. (2015), the time derivative could have been approximated using other numerically more robust methods. However, the method to calculate the time derivative of streamflow may not have a large impact on our subsequent feature importance analyses and the conclusions made, given the comparative large sample hydrology nature of our study.

We acknowledge that some of the climatic attributes used in our analyses, including snowmelt and actual evapotranspiration, are modelled output and are prone to model uncertainty. Particularly, the snowmelt data released by Era5-Land is not sufficiently validated against field data and therefore is inherently uncertain. Additionally, our feature importance analyses did not include all important climatic attributes controlling recession behaviours, including soil temperature (proxy for seasonally frozen ground) which could impact streamflow generation mechanisms in snow-dominated catchments. Future work should focus on developing more robust databases on snowmelt, evapotranspiration and seasonally frozen ground in order to sufficiently quantify the importance of all climatic attributes controlling recession behaviours.

By considering a large variety of process-motivated climatic and physical attributes, we roughly incorporated mechanistic linkages between subsurface water storage and release in a statistical framework. For instance, we detected the underlying unique streamflow recession behaviour related to detailed snow water storage characteristics in snow-dominated catchments and the dominance of catchment steepness and belowground properties on recession behaviour in rain-dominated catchments. The former is a crucial step toward assessing catchment sensitivity to climate change as snow storage characteristics could be significantly impacted (Harpold et al., 2015; Harpold & Brooks, 2018; Musselman et al., 2017). Nevertheless, random forests model, or other statistical tools, cannot identify (and learn) all physical processes related to snowmelt and hydrologic flowpaths. Indeed, as a “black box” machine learning algorithm, random forests cannot identify all “true” scientific interactions among the process-motivated predictors we used, in explaining catchment recession behaviour. To improve the capability of modern statistical learning tools, one must combine the statistical approaches with strong hydrologically based reasoning and carefully choose the predictors which best represent catchment hydrologic functions and processes (as recently done in Janssen & Ameli, 2021).

## 6 | CONCLUSION

We introduced a newly developed statistical feature importance approach, in combination with random forests, to identify the physical and climatic drivers of hydrograph recession behaviour across 1033 catchments in the United States and Canada. Our results showed the

dominance of climatic attributes in driving recession instability ( $\log(a)$ ), regardless of the catchment size and their dominant precipitation type. Additionally, our results suggested that streamflow recession behaviour, particularly recession nonlinearity, strongly depends on belowground attributes and slope in rain-dominated medium size catchments, and strongly depend on slope and how snow accumulates, and when it melts, in snow-dominated medium size catchments. Indeed, a suite of catchment soil/geological attributes strongly controlled recession nonlinearity in rain-dominated medium size (50–1000 km<sup>2</sup>) catchments, while such relative dominance over climatic attributes reduces as scale increased and/or the dominant precipitation type varied to snowfall. We also showed the random forests' efficiency in the extrapolation of the prediction of recession parameters to the ungauged basins, using four hypothetical gauging scenarios. Our findings on the influences of the precipitation type and detailed snowmelt related attributes on catchment recession behaviours can help us better assess catchments vulnerabilities in a fast-changing climate with a potentially larger fraction of precipitation as rain (rather than snow) as well as shallower snow depths in future.

## AUTHOR CONTRIBUTIONS

Hongyi Li conducted the statistical analyses and drafted the manuscript. Ali Ameli developed the scientific concept of the study and edited the manuscript.

## ACKNOWLEDGEMENTS

This research was funded by the grant awarded to Ali Ameli by NSERC-Funded Canadian Statistical Science Institute (CANSSI). Kim Janzen, at the University of Saskatchewan, is thanked for assistance with the final manuscript editing. Joe Janssen, at the University of British Columbia, is thanked for providing MCI code. We thank three reviewers of *Hydrological Processes* journal for their constructive comments.

## DATA AVAILABILITY STATEMENT

Canadian gauges from the HYDAT dataset released by the Water Survey Canada is available at <https://www.canada.ca/en/environment-climate-change/services/water-overview/quantity/monitoring/survey/data-products-services/national-archive-hydat.html> and 671 United States stream gauges from the CAMELS dataset (Addor et al., 2017) is freely available at <https://ral.ucar.edu/solutions/products/camels>. The ERA5-Land (Muñoz-Sabater et al., 2021) hourly and monthly data used for this study are available through the Climate Data Store, <https://doi.org/10.24381/cds.e2161bac> and <https://doi.org/10.24381/cds.68d2bb30>, respectively. Flow direction and flow accumulation data from MERIT Hydro database (Yamazaki et al., 2019) are available at [http://hydro.iis.u-tokyo.ac.jp/~yamadai/MERIT\\_Hydro/](http://hydro.iis.u-tokyo.ac.jp/~yamadai/MERIT_Hydro/). The soil hydraulic properties from a global-scale database developed by Dai et al. (2019) are freely accessible at <http://globalchange.bnu.edu.cn/research>. Global-scale bedrock permeability is freely available by contacting the corresponding author of Gleeson et al. (2014).

## ORCID

Hongyi Li  <https://orcid.org/0000-0001-9279-9224>

Ali Ameli  <https://orcid.org/0000-0002-8173-887X>

## REFERENCES

- Addor, N., Nearing, G., Prieto, C., Newman, A. J., Le Vine, N., & Clark, M. P. (2018). A ranking of hydrological signatures based on their predictability in space. *Water Resources Research*, 54(11), 8792–8812.
- Addor, N., Newman, A. J., Mizukami, N., & Clark, M. P. (2017). The CAMELS data set: Catchment attributes and meteorology for large-sample studies. *Hydrology and Earth System Sciences*, 21(10), 5293–5313.
- Ameli, A. A., Craig, J. R., & McDonnell, J. J. (2015). Are all runoff processes the same? Numerical experiments comparing a Darcy-Richards solver to an overland flow-based approach for subsurface storm runoff simulation. *Water Resources Research*, 51(12), 10008–10028.
- Basso, S., Schirmer, M., & Botter, G. (2015). On the emergence of heavy-tailed streamflow distributions. *Advances in Water Resources*, 82, 98–105.
- Berghuijs, W. R., Hartmann, A., & Woods, R. A. (2016). Streamflow sensitivity to water storage changes across Europe. *Geophysical Research Letters*, 43(5), 1980–1987. <https://doi.org/10.1002/2016gl067927>
- Berghuijs, W. R., Woods, R. A., & Hrachowitz, M. (2014). A precipitation shift from snow towards rain leads to a decrease in streamflow. *Nature Climate Change*, 4(7), 583–586.
- Biswal, B., & Marani, M. (2010). Geomorphological origin of recession curves. *Geophysical Research Letters*, 37(24), L24403. <https://doi.org/10.1029/2010gl045415>
- Blöschl, G., Sivapalan, M., Wagener, M., Viglione, A., & Savenije, H. (2014). *Runoff prediction in ungauged basins*. Cambridge University Press.
- Brutsaert, W. (2005). *Hydrology: An introduction*. Cambridge University Press.
- Brutsaert, W., & Nieber, J. L. (1977). Regionalized drought flow hydrographs from a mature glaciated plateau. *Water Resources Research*, 13(3), 637–643.
- Buttle, J. M. (2018). Mediating stream baseflow response to climate change: The role of basin storage. *Hydrological Processes*, 32(3), 363–378. <https://doi.org/10.1002/hyp.11418>
- Catav, A., Fu, B., Ernst, J., Sankararaman, S., Gilad-Bachrach, R., 2020. Marginal contribution feature importance—An axiomatic approach for the natural case. arXiv preprint arXiv:2010.07910.
- Chen, B., & Krajewski, W. (2016). Analysing individual recession events: Sensitivity of parameter determination to the calculation procedure. *Hydrological Sciences Journal*, 61(16), 2887–2901.
- Clark, M. P., Rupp, D. E., Woods, R. A., Tromp-van Meerveld, H. J., Peters, N. E., & Freer, J. E. (2009). Consistency between hydrological models and field observations: Linking processes at the hillslope scale to hydrological responses at the watershed scale. *Hydrological Processes: An International Journal*, 23(2), 311–319.
- Clow, D. W. (2010). Changes in the timing of snowmelt and streamflow in Colorado: A response to recent warming. *Journal of Climate*, 23(9), 2293–2306.
- Dai, Y., Xin, Q., Wei, N., Zhang, Y., Shangguan, W., Yuan, H., & Lu, X. (2019). A global high-resolution data set of soil hydraulic and thermal properties for land surface modeling. *Journal of Advances in Modeling Earth Systems*, 11(9), 2996–3023.
- Davenport, F. V., Herrera-Estrada, J. E., Burke, M., & Diffenbaugh, N. S. (2020). Flood size increases nonlinearly across the western United States in response to lower snow-precipitation ratios. *Water Resources Research*, 56(1), e2019WR025571.
- Ding, Y., Kong, J., Zhang, J., Luo, Z., Shen, C., Lu, C., & Dong, X. (2021). On the use of modified Boussinesq equation for studying double-layered hillslope recession characteristics. *Journal of Hydrology*, 603, 127041.

- Dralle, D. N., Boisramé, G. F. S., & Thompson, S. E. (2014). Spatially variable water table recharge and the hillslope hydrologic response: Analytical solutions to the linearized hillslope Boussinesq equation. *Water Resources Research*, 50(11), 8515–8530.
- Dralle, D. N., Karst, N. J., Charalampous, K., Veenstra, A., & Thompson, S. E. (2017). Event-scale power law recession analysis: Quantifying methodological uncertainty. *Hydrology and Earth System Sciences*, 21(1), 65–81.
- Ghosh, D. K., Wang, D., & Zhu, T. (2016). On the transition of base flow recession from early stage to late stage. *Advances in Water Resources*, 88, 8–13.
- Gleeson, T., Moosdorf, N., Hartmann, J., & Beek, L. P. H. (2014). A glimpse beneath earth's surface: GLobal HYdrogeology MaPS (GLHYMPS) of permeability and porosity. *Geophysical Research Letters*, 41(11), 3891–3898.
- Godsey, S. E., Kirchner, J. W., & Tague, C. L. (2014). Effects of changes in winter snowpacks on summer low flows: Case studies in the Sierra Nevada, California, USA. *Hydrological Processes*, 28(19), 5048–5064. <https://doi.org/10.1002/hyp.9943>
- Hammond, J. C., Harpold, A. A., Weiss, S., & Kampf, S. K. (2019). Partitioning snowmelt and rainfall in the critical zone: Effects of climate type and soil properties. *Hydrology and Earth System Sciences*, 23(9), 3553–3570.
- Hammond, J. C., Saavedra, F. A., & Kampf, S. K. (2018). How does snow persistence relate to annual streamflow in mountain watersheds of the western US with wet maritime and dry continental climates? *Water Resources Research*, 54(4), 2605–2623.
- Harman, C. J., Sivapalan, M., & Kumar, P. (2009). Power law catchment-scale recessions arising from heterogeneous linear small-scale dynamics. *Water Resources Research*, 45(9), W09404. <https://doi.org/10.1029/2008WR007392>
- Harpold, A. A., & Brooks, P. D. (2018). Humidity determines snowpack ablation under a warming climate. *Proceedings of the National Academy of Sciences*, 115(6), 1215–1220.
- Harpold, A. A., Molotch, N. P., Musselman, K. N., Bales, R. C., Kirchner, P. B., Litvak, M., & Brooks, P. D. (2015). Soil moisture response to snowmelt timing in mixed-conifer subalpine forests. *Hydrological Processes*, 29(12), 2782–2798.
- Hazenberg, P., Fang, Y., Broxton, P., Gochis, D., Niu, G.-Y., Pelletier, J. D., & Zeng, X. (2015). A hybrid-3D hillslope hydrological model for use in earth system models. *Water Resources Research*, 51(10), 8218–8239.
- Hopp, L., & McDonnell, J. J. (2009). Connectivity at the hillslope scale: Identifying interactions between storm size, bedrock permeability, slope angle and soil depth. *Journal of Hydrology*, 376(3–4), 378–391. <https://doi.org/10.1016/j.jhydrol.2009.07.047>
- Huscroft, J., Gleeson, T., Hartmann, J., & Börker, J. (2018). Compiling and mapping global permeability of the unconsolidated and consolidated earth: GLobal HYdrogeology MaPS 2.0 (GLHYMPS 2.0). *Geophysical Research Letters*, 45(4), 1897–1904. <https://doi.org/10.1002/2017gl075860>
- Huyck, A. A. O., Pauwels, V. R. N., & Verhoest, N. E. C. (2005). A base flow separation algorithm based on the linearized Boussinesq equation for complex hillslopes. *Water Resources Research*, 41(8), W08415. <https://doi.org/10.1029/2004WR003789>
- Jachens, E. R., Rupp, D. E., Roques, C., & Selker, J. S. (2020). Recession analysis revisited: Impacts of climate on parameter estimation. *Hydrology and Earth System Sciences*, 24(3), 1159–1170.
- Janssen, J., & Ameli, A. A. (2021). A hydrologic functional approach for improving large-sample hydrology performance in poorly-gauged regions. *Water Resources Research*, 57(9), e2021WR030263.
- Jasechko, S., Perrone, D., Seybold, H., Fan, Y., & Kirchner, J. W. (2020). Groundwater level observations in 250,000 coastal US wells reveal scope of potential seawater intrusion. *Nature Communications*, 11(1), 1–9.
- Jehn, F. U., Bestian, K., Breuer, L., Kraft, P., & Houska, T. (2020). Using hydrological and climatic catchment clusters to explore drivers of catchment behavior. *Hydrology and Earth System Sciences*, 24(3), 1081–1100.
- Jung, Y. (2018). Multiple predicting K-fold cross-validation for model selection. *Journal of Nonparametric Statistics*, 30(1), 197–215.
- Karlsen, R. H., Bishop, K., Grabs, T., Ottosson-Löfvenius, M., Laudon, H., & Seibert, J. (2019). The role of landscape properties, storage and evapotranspiration on variability in streamflow recessions in a boreal catchment. *Journal of Hydrology*, 570, 315–328.
- Kirchner, J. W. (2009). Catchments as simple dynamical systems: Catchment characterization, rainfall-runoff modeling, and doing hydrology backward. *Water Resources Research*, 45(2), W02429. <https://doi.org/10.1029/2008WR006912>
- Li, H.-Y., Sivapalan, M., Tian, F., & Harman, C. (2014). Functional approach to exploring climatic and landscape controls of runoff generation: 1. Behavioral constraints on runoff volume. *Water Resources Research*, 50(12), 9300–9322. <https://doi.org/10.1002/2014wr016307>
- Luo, Z., Shen, C., Kong, J., Hua, G., Gao, X., Zhao, Z., & Li, L. (2018). Effects of unsaturated flow on hillslope recession characteristics. *Water Resources Research*, 54(3), 2037–2056.
- Marçais, J., De Dreuzy, J.-R., & Erhel, J. (2017). Dynamic coupling of subsurface and seepage flows solved within a regularized partition formulation. *Advances in Water Resources*, 109, 94–105.
- May, C. L., & Lee, D. C. (2004). The relationships among in-channel sediment storage, pool depth, and summer survival of juvenile salmonids in Oregon coast range streams. *North American Journal of Fisheries Management*, 24(3), 761–774.
- McCabe, G. J., Wolock, D. M., & Valentin, M. (2018). Warming is driving decreases in snow fractions while runoff efficiency remains mostly unchanged in snow-covered areas of the western United States. *Journal of Hydrometeorology*, 19(5), 803–814.
- McDonnell, J. J., Sivapalan, M., Vaché, K., Dunn, S., Grant, G., Haggerty, R., & Weiler, M. (2007). Moving beyond heterogeneity and process complexity: A new vision for watershed hydrology. *Water Resources Research*, 43(7), n/a-n/a. <https://doi.org/10.1029/2006wr005467>
- Muñoz-Sabater, J., Dutra, E., Agustí-Panareda, A., Albergel, C., Arduini, G., Balsamo, G., & Hersbach, H. (2021). ERA5-land: A state-of-the-art global reanalysis dataset for land applications. *Earth System Science Data Discussions*, 13(9), 4349–4383.
- Musselman, K. N., Clark, M. P., Liu, C., Ikeda, K., & Rasmussen, R. (2017). Slower snowmelt in a warmer world. *Nature Climate Change*, 7(3), 214–219.
- Mutzner, R., Bertuzzo, E., Tarolli, P., Weijs, S. V., Nicotina, L., Ceola, S., & Rinaldo, A. (2013). Geomorphic signatures on Brutsaert base flow recession analysis. *Water Resources Research*, 49(9), 5462–5472.
- Paniconi, C., Troch, P. A., van Loon, E. E., & Hilberts, A. G. J. (2003). Hillslope-storage Boussinesq model for subsurface flow and variable source areas along complex hillslopes: 2. Intercomparison with a three-dimensional Richards equation model. *Water Resources Research*, 39(11), 1317. <https://doi.org/10.1029/2002WR001730>
- Ranjram, M., & Craig, J. R. (2021). Use of an efficient proxy solution for the hillslope-storage Boussinesq problem in upscaling of subsurface stormflow. *Water Resources Research*, 57(4), e2020WR029105.
- Roques, C., Rupp, D. E., & Selker, J. S. (2017). Improved streamflow recession parameter estimation with attention to calculation of  $-dQ/dt$ . *Advances in Water Resources*, 108, 29–43.
- Rupp, D. E., & Selker, J. S. (2005). Drainage of a horizontal Boussinesq aquifer with a power law hydraulic conductivity profile. *Water Resources Research*, 41(11), W11422. <https://doi.org/10.1029/2005WR004241>
- Rupp, D. E., & Selker, J. S. (2006). On the use of the Boussinesq equation for interpreting recession hydrographs from sloping aquifers. *Water*

- Resources Research, 42(12), W12421. <https://doi.org/10.1029/2006WR005080>
- Shangguan, W., Hengl, T., Mendes de Jesus, J., Hua, Y., & Dai, Y. (2017). Mapping the global depth to bedrock for land surface modeling. *Journal of Advances in Modeling Earth Systems*, 9(1), 65–88.
- Shaw, S. B., & Riha, S. J. (2012). Examining individual recession events instead of a data cloud: Using a modified interpretation of  $dQ/dt-Q$  streamflow recession in glaciated watersheds to better inform models of low flow. *Journal of Hydrology*, 434, 46–54.
- Stein, L., Clark, M. P., Knoben, W. J. M., Pianosi, F., & Woods, R. A. (2021). How do climate and catchment attributes influence flood generating processes? A large-sample study for 671 catchments across the contiguous USA. *Water Resources Research*, 57(4), e2020WR028300.
- Tashie, A., Pavelsky, T., & Band, L. E. (2020a). An empirical reevaluation of streamflow recession analysis at the continental scale. *Water Resources Research*, 56(1), e2019WR025448.
- Tashie, A., Pavelsky, T., & Emanuel, R. E. (2020b). Spatial and temporal patterns in baseflow recession in the continental United States. *Water Resources Research*, 56(3), e2019WR026425.
- Tashie, A., Scaife, C. I., & Band, L. E. (2019). Transpiration and subsurface controls of streamflow recession characteristics. *Hydrological Processes*, 33(19), 2561–2575.
- Thomas, B. F., Vogel, R. M., & Famiglietti, J. S. (2015). Objective hydrograph baseflow recession analysis. *Journal of Hydrology*, 525, 102–112. <https://doi.org/10.1016/j.jhydrol.2015.03.028>
- Troch, P. A., Berne, A., Bogaart, P., Harman, C., Hilberts, A. G. J., Lyon, S. W., & Selker, J. S. (2013). The importance of hydraulic groundwater theory in catchment hydrology: The legacy of Wilfried Brutsaert and Jean-Yves Parlange. *Water Resources Research*, 49(9), 5099–5116.
- Troch, P. A., Paniconi, C., & van Loon, E. (2003). Hillslope-storage Boussinesq model for subsurface flow and variable source areas along complex hillslopes: 1. Formulation and characteristic response. *Water Resources Research*, 39(11), 1316. <https://doi.org/10.1029/2002WR001728>
- Vogel, R. M., & Kroll, C. N. (1992). Regional geohydrologic-geomorphic relationships for the estimation of low-flow statistics. *Water Resources Research*, 28(9), 2451–2458.
- Woo, M.-k., Thorne, R., Szeto, K., & Yang, D. (2008). Streamflow hydrology in the boreal region under the influences of climate and human interference. *Philosophical Transactions of the Royal Society B: Biological Sciences*, 363(1501), 2249–2258.
- Woods, R. A. (2009). Analytical model of seasonal climate impacts on snow hydrology: Continuous snowpacks. *Advances in Water Resources*, 32(10), 1465–1481.
- Wu, S., Zhao, J., Wang, H., & Sivapalan, M. (2021). Regional patterns and physical controls of streamflow generation across the conterminous United States. *Water Resources Research*, 57(6), e2020WR028086.
- Yamazaki, D., Ikeshima, D., Sosa, J., Bates, P. D., Allen, G. H., & Pavelsky, T. M. (2019). MERIT hydro: A high-resolution global hydrography map based on latest topography dataset. *Water Resources Research*, 55(6), 5053–5073.
- Ye, S., Li, H.-Y., Huang, M., Ali, M., Leng, G., Leung, L. R., & Sivapalan, M. (2014). Regionalization of subsurface stormflow parameters of hydrologic models: Derivation from regional analysis of streamflow recession curves. *Journal of Hydrology*, 519, 670–682.

## SUPPORTING INFORMATION

Additional supporting information can be found online in the Supporting Information section at the end of this article.

**How to cite this article:** Li, H., & Ameli, A. (2022). A statistical approach for identifying factors governing streamflow recession behaviour. *Hydrological Processes*, 36(10), e14718. <https://doi.org/10.1002/hyp.14718>